Nano-optomechanical Actuator and Pull-Back Instability

Min Ren,[†,§] Jianguo Huang,[‡] Hong Cai,[§] Julius Minglin Tsai,[§] Jinxiong Zhou,[‡] Zishun Liu,[‡] Zhigang Suo,[‡,⊥,*] and Ai-Qun Liu[†,‡,§,*]

[†]School of Electrical and Electronic Engineering, Nanyang Technological University, 50 Nanyang Avenue, Singapore 639798, [‡]Xi'an Jiao Tong University, Xian Ning West Road No. 28, Xi an, China 710049, [§]Institute of Microelectronics, A*STAR, 11 Science Park Road, Singapore 117685, and [⊥]School of Engineering and Applied Sciences, Harvard University, Cambridge, Massachusetts 02138, United States

ABSTRACT This paper studies the nonlinear behavior of a nano-optomechanical actuator, consisting of a free-standing arc in a ring resonator that is coupled to a bus waveguide through evanescent waves. The arc deflects when a control light of a fixed wavelength and optical power is pumped into the bus waveguide, while the amount of deflection is monitored by measuring the transmission spectrum of a broadband probe light. This nanoactuator achieves a maximal deflection of 43.1 nm, with a resolution of 0.28 nm. The optical force is a nonlinear function of the deflection of the arc, leading to pull-back instability when the control light is red-tuned. This instability is studied by a combination of experiment and modeling. Potential applications of the nanoactuator include bio-nanomotor, optical switches, and optomechanical memories.

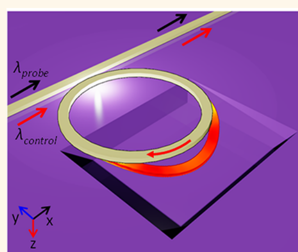

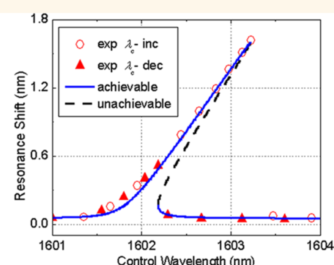

KEYWORDS: nanoelectromechanical systems · nanoactuator · pull-back effect · optical force

Silicon-based microelectromechanical systems (MEMS) use diverse methods of actuation, such as piezoelectrics,[1] thermal expansion,[2] electromagnetic interactions,[3] surface acoustic waves,[4] and electrostatics.[5,6] The MEMS actuators enable on-chip integration with high reliability and low cost. However, the microscale dimensions limit both the speed and precision of actuation.

Nanoelectromechanical systems (NEMS) scale down the dimensions.[7,8] In particular, NEMS employing electrostatic forces have been developed.[9,10] For parallel-plate electrostatic actuators, the pull-in instability occurs at $^1/_3$ of the plate−plate distance.[5,6,11] This nonlinear phenomenon may limit the stable range of actuation, or be used as switches and relays. As the width and length of the capacitive actuators are scaled down to nanometers, the capacitance decreases. The small capacitance increases the impedance, making the devices susceptible to RF noise, and limiting their applications for high-precision sensing or high-resolution actuation.

Of particular interest is a new method of actuation enabled by NEMS: optical forces[12−15] can realize nanoscale positioning compatible to high-density, on-chip integration. In a guided-wave structure, an optical force is exerted on the free-standing waveguide when the guided light is evanescently coupled to a nearby waveguide or to a dielectric substrate.[16−20] The amplitude of the optical force depends on the gradient of the electromagnetic field. As the waveguides are scaled down to nanosize, the optical force can be increased to several pN/mW. A ring resonator[21] with high quality factor is utilized to enhance the gradient optical force, enabling manipulation of optical response at a relatively low light power.[22,23]

Here we study the nonlinear behavior of a nano-optomechanical actuator, consisting of a free-standing arc in a ring and a bus waveguide. When a monochromatic control light is pumped into the bus waveguide, the ring is coupled with the bus waveguide and the dielectric substrate through evanescent waves. The resonant frequency shifts when the arc deflects, and the gradient of the optical energy with respect to the deflection of the arc defines the optical force. The elasticity of the arc gives rise to the mechanical force that resists deflection. When the optical force balances the mechanical force,

* Address correspondence to suo@seas.harvard.edu, eaqliu@ntu.edu.sg.

Received for review December 7, 2012 and accepted January 22, 2013.

Published online January 25, 2013
10.1021/nn3056687

© 2013 American Chemical Society

the arc reaches an equilibrium shape. The amount of deflection is monitored by measuring the transmission spectrum of a broadband probe light in the waveguide. The optical force is a nonlinear function of the deflection, leading to pull-back instability when the control light is red-tuned. This nonlinear behavior is studied by comparing the experimental measurement with finite element simulation.

RESULTS AND DISCUSSION

Both the ring resonator and the bus waveguide are 450 nm in width and 220 nm in height (Figure 1). The gap between the ring resonator and the bus waveguide is 200 nm. An air gap between the free-standing arc and the silicon dioxide (SiO_2) layer is $g_0 = 160$ nm. A cross-sectional length of the arc is 11.2 μm. We inject into the bus waveguide a broadband probe light and a control light. The probe light is low-power and broadband, and is used to detect the deflection of the arc. The control light is high-power and monochromatic, and is used to generate optical force to deflect the arc. When the arc bends with a central deflection x, the air gap is changed to $g = g_0 - x$.

The effective refractive index of the arc increases when the arc is bended down to the SiO_2 layer. Consequently, the resonant wavelength λ_r is red-shifted, $\lambda_r = \lambda_{r0} + \delta\lambda_r$, where λ_{r0} is the resonant wavelength before bending, and $\delta\lambda_r$, is the shift of the resonant wavelength. We calculate the resonant wavelength for various air gaps using the commercial software RSOFT (Figure 2a), and fit the optomechanical wavelength tuning coefficient to $\partial\lambda_r/\partial x = A_1 \cdot \exp(A_2 x)$, where $A_1 = 2.3 \times 10^{-2}$ and $A_2 = 1.35 \times 10^{-2}$ at $g =$ 160 nm. Thus the deflection x can be indirectly monitored by the shift of the resonant wavelength $\delta\lambda_r$ in the transmission spectrum. This offers an effective method to detect the nanoscale displacement.

The optical energy stored in the ring resonator can be expressed as[21]

$$U = \frac{2\tau_e^{-1}P_{in}}{((\lambda_c - \lambda_r)2\pi c\lambda_r^{-2})^2 + (\tau_i^{-1} + \tau_e^{-1})^2} \quad (1)$$

where P_{in} is the power of the control light pumped into the bus waveguide, $1/\tau_e$ the extrinsic decay rate due to the externally coupling of the transmitted wave, $1/\tau_i$ the intrinsic decay rate due to the internal cavity loss, λ_c the wavelength of the control light, and λ_r the resonant wavelength.

The derivative of the optical energy with respect to the gap gives the gradient optical force.[13] The optical force exerted on the arc is given by

$$\begin{aligned} F_{opt} &= -\frac{\partial U}{\partial g} = -\frac{U}{\lambda_r}\frac{\partial \lambda_r}{\partial x} \\ &= -\frac{2\tau_e^{-1}P_{in}}{(\lambda_c - \lambda_r)^2(2\pi c)^2\lambda_r^{-3} + \lambda_r(\tau_i^{-1} + \tau_e^{-1})^2}\frac{\partial \lambda_r}{\partial x} \end{aligned} \quad (2)$$

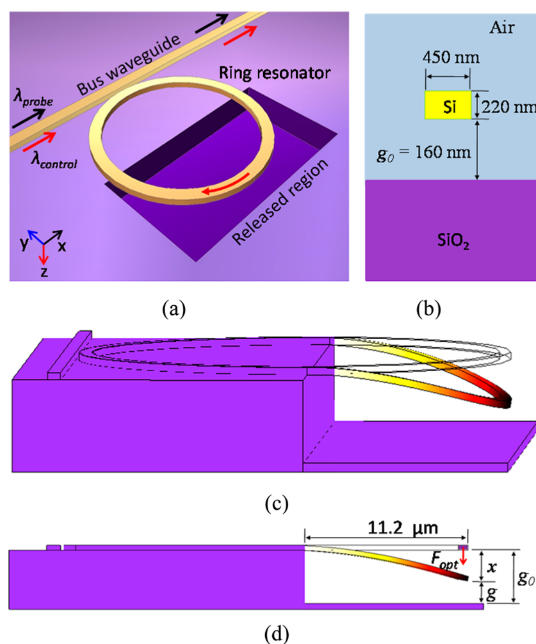

Figure 1. (a) The schematic of the nanoactuator; (b) the cross-sectional view of the free-standing arc; (c) the optical force causes the arc to deflect; (d) the cross-sectional view of the deflected actuator.

Subject to a control light of a fixed wavelength and power, the optical force is a nonlinear function of the deflection, $F_{opt}(x)$. This nonlinear function is plotted in Figure 2b for several levels of detuning, defined by the difference between the wavelength of the control light and resonant wavelength of the unbent arc, $\Delta = \lambda_c - \lambda_{r0}$. The nonlinearity of gradient optical force results from the interaction between the mechanical motion and the optical field. Owing to the cavity effect of the ring resonator, the optical force depends on the resonant wavelength, when the power and wavelength of the control light is constant. The deflection of the arc modifies the effective refractive index and thus tunes the resonant wavelength of the ring. Consequently, the deflection provides a "feedback" to the amount of the optical force, and the function $F_{opt}(x)$ is nonmonotonic. When the control light of a fixed wavelength and power is pumped into the bus waveguide, the optical force increases as the deflection of the arc tunes the resonant wavelength of the ring toward the wavelength of the control light, and the optical force decreases when the deflection of the arc tunes the resonant wavelength of the ring away from the wavelength of the control light. The dominant part in eq 2 is $(\lambda_c - \lambda_r)^2(2\pi c)^2\lambda_r^{-3} \approx (\lambda_c - \lambda_r)^2(2\pi c)^2\lambda_{r0}^{-3}$. As the deflection of the arc increases, the value of $(\lambda_c - \lambda_r)^2$ decreases to zero and then increases again. Thus the curve of $|F_{opt}|$ *vs* x is quasi-Lorentzian, which reaches a maximum value at about $\lambda_r(x) = \lambda_c$. The curve is asymmetrical with respect to the peak point because the optomechanical wavelength tuning coefficient varies with the deflection.

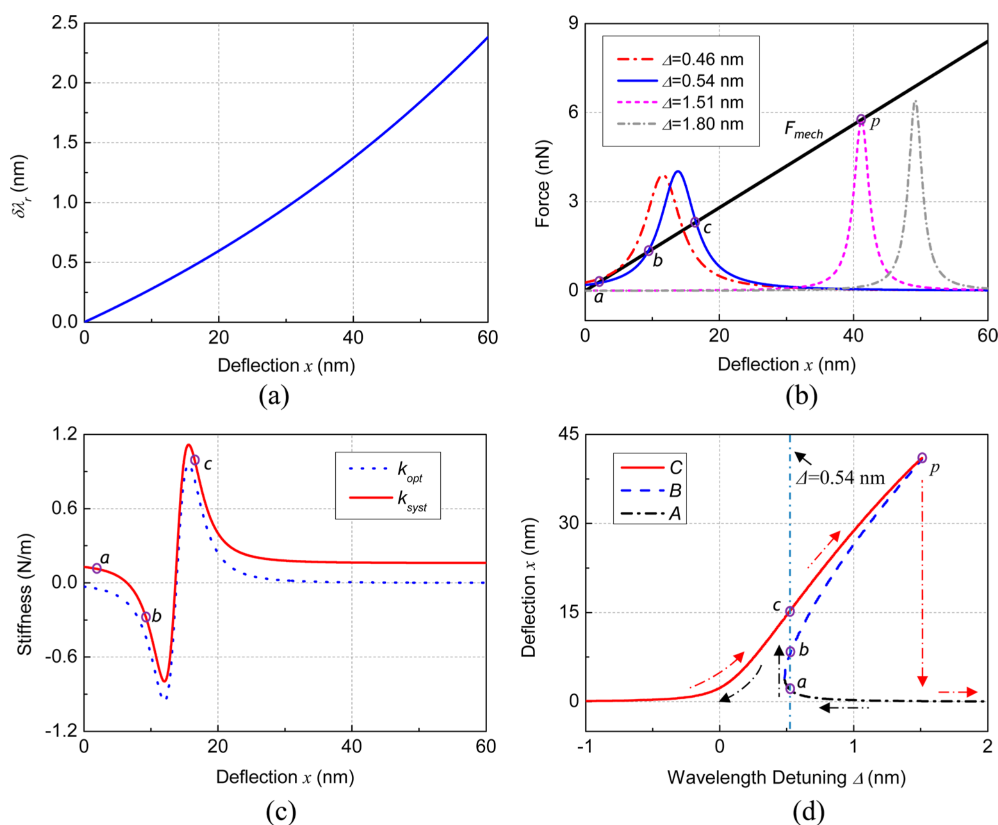

Figure 2. Simulation of (a) the shift of the resonant wavelength as a function of the deflection; (b) comparison of optical force and mechanical force under different wavelength detuning conditions; (c) optical spring and system stiffness *vs* *x* when $\Delta = 0.54$ nm; (d) nonlinear relation between the deflection of the arc and the wavelength of the control light (represented by the detuning Δ).

The defection of the arc can be varied by changing either the wavelength λ_c or the power P_{in} of the control light. We decide to vary λ_c in this paper for two reasons. First, varying the wavelength of the control light provides an efficient positioning control using the square relation between x and Δ (based on eq 2, $x \propto F_{opt}(x) \propto (\lambda_c - \lambda_r)^{-2}$, while $x \propto (P_{in})^1$). Second, this approach avoids fluctuation of power variations.

Once the arc deflects, the elasticity of the arc gives rise to a mechanical force, F_{mech}, that tends to pull the arc back to its original position. There are two forces in this system: the mechanical force is linear in and the optical force is nonlinear in the deflection. The two forces balance each other at the equilibrium points. The linear force becomes too large to be balanced by the nonlinear force when the deflection is above a certain value, which results in the pull-back instability. The mechanical spring constant of the arc is k_{mech} = 0.14 N/m, which is calculated by using the finite-element software COMSOL. The shape of the arc reaches a state of equilibrium when the optical force balances the mechanical force:

$$F_{opt}(x) + k_{mech}x = 0 \quad (3)$$

Because the optical force is a nonlinear function of the deflection, for the control light of a fixed wavelength, the arc may deflect to multiple states of equilibrium. In Figure 2b, when the optical power is P_{in} = 2.8 mW, the curve of $|F_{opt}|$ under $\Delta = 0.54$ nm is highlighted. The two curves (F_{mech} and $|F_{opt}|$) intersect at three points, *a*, *b*, and *c*. When $\Delta = 0.46$ nm, points *a* and *b* merge to a single point. When $\Delta < 0.46$ nm, the merged point disappears, and only one state of equilibrium *c* still exists. Consequently, as the wavelength of the control light reduces, the arc will undergo a pull-in instability, jumping toward state *c*. On the other hand, when Δ increases, points *b* and *c* move closer, while point *a* approaches to zero-deflection position. At a critical detuning value of $\Delta = 1.51$ nm, points *b* and *c* merge (at the stable point *p*). At point *p*, the largest deflection, x_p = 40.8 nm is obtained. When $\Delta > 1.51$ nm, the situation of $F_{mech} > |F_{opt}|$ is always satisfied, therefore the largest deflection is not maintainable and the free-standing arc will be pulled back to point *a*, which is nearly at the initial status of $x = 0$ nm. This phenomenon is called pull-back instability. Therefore, the actuation of the free-standing arc is controllable when $x \leq x_p$. The normalized controllable actuation range is $x_p/g_0 = 25.5\%$.

To analyze the stability of these states of equilibrium, we invoke the concept of optical spring[24,25] and system stiffness.[26] By analogy with the mechanical stiffness, the stiffness of the optical spring is defined by $k_{opt} = \partial F_{opt}/\partial x$. According to eq 2, the stiffness of the optical spring can

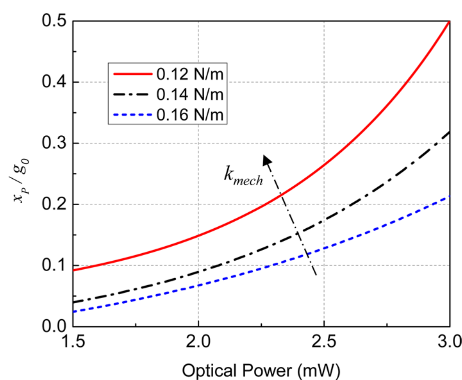

Figure 3. The dependence of normalized pull-back displacement on optical power and mechanical spring constant of the arc.

be expressed as

$$k_{\rm opt} = \frac{U}{\lambda_{\rm r0}^2}\left(2\left(\frac{\partial\lambda_{\rm r}}{\partial x}\right)^2 - \lambda_{\rm r0}\frac{\partial^2\lambda_{\rm r}}{\partial x^2}\right) \quad (4)$$

The optical spring can either "harden" or "soften" the free-standing arc by modifying the intrinsic mechanical spring constant. The system stiffness of the arc is expressed as $k_{\rm syst} = k_{\rm mech} + k_{\rm opt}$. An equilibrium position with negative stiffness ($k_{\rm syst} < 0$) is unstable[26] because it has higher positive stored energy compared to neighboring possible equilibrium positions. When a state of equilibrium is stable, a positive system stiffness is expressed as

$$k_{\rm syst} = k_{\rm mech} + \frac{U}{\lambda_{\rm r0}^2}\left(2\left(\frac{\partial\lambda_{\rm r}}{\partial x}\right)^2 - \lambda_{\rm r0}\frac{\partial^2\lambda_{\rm r}}{\partial x^2}\right) > 0 \quad (5)$$

When eq 2 and 3 are substituted into eq 5, the stable condition for an equilibrium state is

$$\lambda_{\rm r}\frac{\partial\lambda_{\rm r}}{\partial x} + 2\left(\frac{\partial\lambda_{\rm r}}{\partial x}\right)^2 x - \lambda_{\rm r}\frac{\partial^2\lambda_{\rm r}}{\partial x^2}x > 0 \quad (6)$$

The variation of $k_{\rm opt}$ and $k_{\rm syst}$ with x under special condition of $\Delta = 0.54$ nm is shown in Figure 2c. The three intersection points are labeled as a, b, and c. Note that $k_{\rm syst} > 0$ at points a and c, corresponding to two stable states of equilibrium. Note that $k_{\rm syst} < 0$ at point b, corresponding to an unstable state of equilibrium.

Figure 2d presents the relation between the deflection x and the detuning Δ. Three different parts of the curve correspond to three types of equilibrium states. Curve C consists of all the stable states of equilibrium like point c, curve B consists of all the unstable states of equilibrium like point b, and curve A consists of all the stable states of equilibrium like point a. These curves suggest a hysteretic behavior. If Δ is increased by changing the wavelength of the control light, the deflection x of the arc follows curve C, until $x_{\rm p}$ (point p) is achieved at the pull-back detuning $\Delta = 1.51$ nm. When $\Delta > 1.51$ nm, the deflection follows curve A. If Δ is decreased, the deflection will follow curve A first until $\Delta = 0.46$ nm, and then the deflection follows curve C.

In this actuator, the pull-back instability dominates the nonlinear behavior of the positioning of the arc.

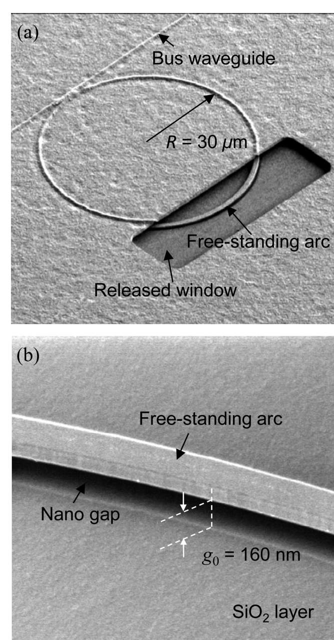

Figure 4. SEM image of (a) the bus waveguide coupled to a partially released ring resonator; (b) the free-standing arc of the ring resonator lies inside of the released window, with the initial gap of 160 nm.

Although the normalized pull-back displacement, $x_{\rm p}/g_0$, is 25.5% under the condition of $P_{\rm in}$ = 2.8 mW and $k_{\rm mech}$ = 0.14 N/m, it can be increased through increasing the optical power $P_{\rm in}$, and decreasing the mechanical spring constant $k_{\rm mech}$, as shown in Figure 3. For example, the value of $x_{\rm p}/g_0$ is expected to be 50% when $P_{\rm in}$ = 3.0 mW and $k_{\rm mech}$ = 0.12 N/m.

When $\partial\lambda_{\rm r}/\partial x = A_1 \exp(A_2 x)$ is substituted into eq 6, the stable condition for an equilibrium state is always satisfied when the initial gap is g_0 = 160 nm ($A_1 = 2.3 \times 10^{-2}$ and $A_2 = 1.35 \times 10^{-2}$). It means that the stable actuation range of the free-standing arc is theoretically able to cover 100% of the nanoair-gap under extremely ideal situations (when $P_{\rm in}$ is ideally increased and $k_{\rm mech}$ is ideally reduced, and the van der Waals force is neglected). Recall that in a parallel-plate capacitive actuator, the pull-in instability occurs when the deflection is $^1/_3$ of its initial gap.

The SEM image of the actuator is shown in Figure 4a. The released window area has a dimension of 65 μm × 15 μm. The zoomed view of the arc inside of the released window is shown in Figure 4b, and the initial gap g_0 between the free-standing arc and the SiO_2 layer is approximately 160 nm.

The measured transmission spectrum of the ring resonator is shown in Figure 5, when a broadband probe light and a control light are coupled into the bus waveguide. The two black dash-lines are the output response for the input probe signal (without control light). Two resonant wavelengths are observed, which are initially at $\lambda_{\rm r0}'$ = 1598.67 nm and $\lambda_{\rm r0}$ = 1601.72 nm, respectively. A 9-dB drop of transmission power at 1601.72 nm is detected. The full width at half-maximum

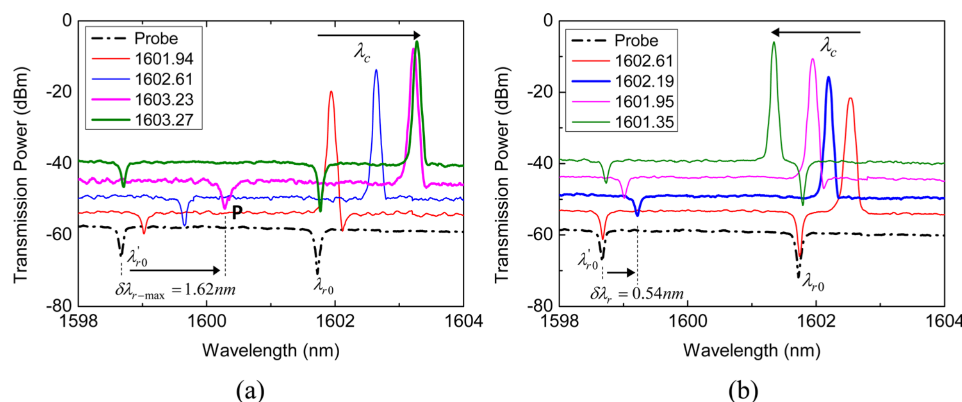

Figure 5. Transmission spectra for control light of several wavelengths: (a) λ_c is increased; (b) λ_c is decreased.

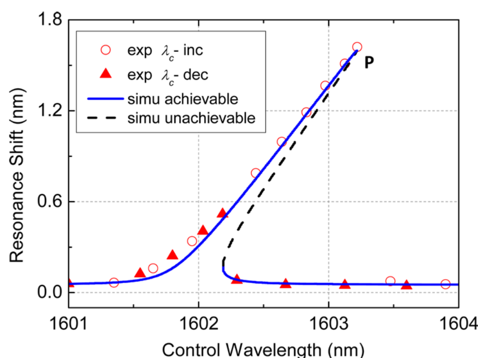

Figure 6. The comparison of simulation and experimental results of the nonlinear actuation, and point P is the pull-back position.

bandwidth of the resonance is 0.055 nm, which corresponds to a loaded quality factor of 2.88 × 10^4, $1/\tau_e$ = 1.18 × 10^{10} Hz and $1/\tau_i$ = 7.25 × 10^9 Hz. When the control light is injected, (λ_c is around λ_{r0}), the shift of the resonant wavelength, $\delta\lambda_r$, is detected on the transmission spectrum. To clearly differentiate the resonance shift while tuning the control wavelength, 4-dBm offset power is set for each optical spectrum.

In Figure 5a, the wavelength λ_c of the control light is increased from the blue detuning side to the red detuning side of λ_{r0}, and the resonance shift $\delta\lambda_r$ increases with λ_c. The resonant wavelength shift $\delta\lambda_{r\text{-max}}$ = 1.62 nm is obtained at λ_c = 1603.23 nm, labeled as point P. Beyond this point, that is, as shown in the curve of λ_c = 1603.27 nm, the resonant wavelength drops to its initial value. The critical point P indicates the pull-back position, where the maximum resonance shift is observed. In Figure 5b, the wavelength λ_c of the control light is decreased from the red detuning side to the blue detuning side of λ_{r0}. The resonant wavelength λ_r is approximately maintained at its initial position until λ_c = 1602.19 nm, where the obvious resonance shift, $\delta\lambda_r$ = 0.54 nm, is observed.

The results of the simulation and experiment are compared in Figure 6. When the control wavelength λ_c is red and blue tuned, two different groups of resonance shift positions are obtained based on the experiments, which correspond to two groups of stable deflection positions (curve *C* and curve *A* in Figure 2d). On the other hand, the unstable points (curve B), are not observed in the experiments. To achieve the pull-back position, λ_c should be increased to track the red shift of the resonant wavelength. The pull-back effect occurs at Δ = 1.51 nm, where the maximum resonance shift is $\delta\lambda_{r\text{-max}}$ = 1.62 nm. According to the simulated optomechanical wavelength tuning coefficient $\partial\lambda_r/\partial x$ = 2.3 × 10^{-2} exp(1.35 × $10^{-2}x$), the corresponding maximum deflection of the arc is 43.1 nm. The positioning resolution of the arc is 0.28 nm, determined by the 0.01 nm tuning step of the wavelength of the control light. Higher resolution is expected by using a tunable laser with smaller tuning step. The experimental results are repeatable with a random range of ±0.04 nm for pull-back wavelength λ_c

CONCLUSIONS

The nano-optomechanical actuator is demonstrated and the pull-back instability is studied by a combination of experiment and modeling. The nanoactuation is controlled through tuning the wavelength of the control light at a fixed power of 2.8 mW. The resolution of the nanoactuation is 0.28 nm within a tuning range of 43.1 nm. The pull-back instability occurs when the control light is red-tuned. This nanoactuator has potential applications for all-optical switches and opto-mechanical memories. Such devices can be achieved by modulating the wavelength of the control light, and can possibly respond at megahertz or even gigahertz. In addition, the nanoactuator may be applied to manipulate nanoscale particles, which requires the combined capability of optical trapping and actuation of the nano-optomechanical actuator.

METHODS

Fabrication of the Nano-actuator. We fabricate the actuator on a silicon-on-insulator (SOI) wafer. Both the ring resonator and the bus waveguide are silicon patterned by reactive-ion-etching (RIE) process. Then 1.5-μm SiO_2 upper cladding layer is deposited onto the silicon waveguide layer. This thickness, sufficient for the high confinement waveguide, forms symmetric cladding

around the silicon waveguide and reduces the transmission loss. A 200-nm silicon nitride is deposited on top of the upper cladding SiO_2 layer, to function as a hard mask during SiO_2 etch. A released window area was defined, inside of which the 200-nm silicon nitride and the 1.5-μm SiO_2 are removed by RIE. Finally, part of the SiO_2 layer underneath the silicon waveguide is etched off by a hydrogen fluoride (HF) vapor etching process and the free-standing arc is formed. The vertical gap between the arc and the remaining SiO_2 layer is controlled by the time of the HF vapor etching process, and other part of the system is protected by the silicon nitride hard mask.

Experimental Setup. In the experiment, both a probe light and a control light are coupled into and out of the bus waveguide (with mode size converter at the tips) through two taper fibers. A polarization controller is used to select only TE light injected into the bus waveguide. The lasing wavelength of the control light is tuned with a step of 0.01 nm and its power is maintained to ensure a 2.8-mW optical power to be injected into the bus waveguide. The probe light is a broadband light ranged from 1535 to 1625 nm, with a power density of −15 dBm/nm. Compared with the control light, the power density of the probe light is weak and does not generate optical force. An optical spectrum analyzer with 0.001-nm resolution is used to measure the transmission spectrum of the ring resonator.

Conflict of Interest: The authors declare no competing financial interest.

REFERENCES AND NOTES

1. Piekarski, B.; Dubey, M.; Devoe, D.; Zakar, E.; Zeto, R.; Conrad, J.; Piekarz, R.; Ervin, M. Fabrication of Suspended Piezoelectric Microresonators. *Integr. Ferroelectr.* **1999**, *24*, 147–154.
2. Lai, Y.; McDonald, J.; Kujath, M.; Hubbard, T. Force Deflection and Power Measurements of Toggled Microthermal Actuators. *J. Micromech. Microengin.* **2004**, *14*, 49–56.
3. Cugat, O.; Delamare, J.; Reyne, G. Magnetic Microactuators and Systems (MAGMAS). *IEEE Trans. Magn.* **2003**, *39*, 3607–3612.
4. Kurosawa, M. K. State-of-the-Art Surface Acoustic Wave Linear Motor and Its Further Applications. *Ultrasonics* **2000**, *38*, 15–19.
5. Fadi, M. A.; Mohammad, I. Y.; Hassen, M. O. On the Nonlinear Resonances and Dynamic Pull-In of Electrostatically Actuated Resonators. *J. Micromech. Microeng.* **2009**, *19*, 045013.
6. Hung, E. S.; Senturia, S. D. Extending the Travel Range of the Analog-Tuned Electrostatic Actuators. *J. Micorelectromech. Syst.* **1999**, *8*, 497–505.
7. Craighead, H. G. Nanoelectromechanical Systems. *Science* **2000**, *290*, 1532–1535.
8. Yang, Y. T.; Callegari, C.; Feng, X. L.; Ekinci, K. L.; Roukes, M. L. Zeptogram-Scale Nanomechanical Mass Sensing. *Nano Lett.* **2006**, *6*, 583–586.
9. Fennimore, A. M.; Yuzvinsky, T. D.; Han, W. Q.; Fuhrer, M. S.; Cumings, J.; Zettl, A. Rotational Actuators Based on Carbon Nanotubes. *Nature* **2003**, *424*, 408–410.
10. He, R. R.; Feng, X. L.; Roukes, M. L.; Yang, P. D. Self-Transducing Silicon Nanowire Electromechanical Systems at Room Temperature. *Nano Lett.* **2008**, *8*, 1756–1761.
11. Bao, M. H. *Analysis and Design Principles of MEMS Devices*; Elsevier: Amsterdam; Oxford, 2005; pp 181−186.
12. Roh, Y. -G.; Tanabe, T.; Shinya, A.; Taniyama, H.; Kuramochi, E.; Matsuo, S.; Sato, T.; Notomi, M. Strong Optomechanical Interaction in a Bilayer Photonic Crystal. *Phys. Rev. B* **2010**, *81*, 121101.
13. Povinelli, M. L.; Lončar, M.; Joannopoulos, J. D. Evanescent-Wave Bonding between Optical Waveguide. *Opt. Lett.* **2005**, *30*, 3042–3044.
14. Jones, P. H.; Palmisano, F.; Bonaccorso, F.; Gucciardi, P. G.; Calogero, G.; Ferrari, A. C.; Marago, O. M. Rotation Detection in Light-Driven Nanorotors. *ACS Nano* **2009**, *3*, 3077–3084.
15. Zhang, J.; Macdonald, K. F.; Zheludev, N. I. Optical Gecko Toe: Optically Controlled Attractive Near-Field Forces between Plasmonic Metamaterials and Dielectric or Metal Surfaces. *Phys. Rev. B* **2012**, *85*, 205123.
16. Tao, J. F.; Wu, J.; Cai, H.; Zhang, Q. X.; Tsai, J. M.; Lin, J. T.; Liu, A. Q. A Nano-machined Optical Logic Gate Driven by Gradient Optical Force. *Appl. Phys. Lett.* **2012**, *100*, 113104.
17. Cai, H.; Xu, K. J.; Liu, A. Q.; Fang, Q.; Yu, M. B.; Lo, G. Q.; Kwong, D. L. Nano-Opto-Mechanical Actuator Driven by Gradient Optical Force. *Appl. Phys. Lett.* **2012**, *100*, 013108.
18. Li, M.; Pernice, W. H. P.; Xiong, C.; Baehr-Jones, T.; Hochberg, M.; Tang, H. X. Harnessing Optical Force in Integrated Photonics Circuits. *Nature* **2008**, *456*, 480–485.
19. Yu, Y. F.; Zhang, J. B.; Bourouina, T.; Liu, A. Q. Optical-Force-Induced Bistability in Nanomachined Ring Resonator Systems. *Appl. Phys. Lett.* **2012**, *100*, 093108.
20. Wiederhecker, G. S.; Chen, L.; Gondarenko, A.; Lipson, M. Controlling Photonics Structures Using Optical Force. *Nature* **2009**, *462*, 633–636.
21. Little, B. E.; Chu, S. T.; Haus, H. A.; Foresi, J.; Laine, J.-P. Microring Resonator Channel Dropping Filters. *J. Lightwave Technol.* **1997**, *15*, 998–1005.
22. Rosenberg, J.; Lin, Q.; Painter, O. Static and Dynamic Wavelength Routing *via* the Gradient Optical Force. *Nat. Photon.* **2009**, *3*, 478–483.
23. Kippenberg, T. J.; Vahala, K. J. Cavity Optomechanics: Back-Action at the Mesoscale. *Science* **2008**, *321*, 1172–1176.
24. Mizrahi, A.; Schächter, L. Two-Slab All-Optical Spring. *Opt. Lett.* **2007**, *32*, 692–694.
25. Singh, S.; Phelps, G. A.; Goldbaum, D. S.; Wright, E. M.; Meystre, P. All-Optical Optomechanics: An Optical Spring Mirror. *Phys. Rev. Lett.* **2010**, *105*, 213602.
26. Lakes, R. S.; Lee, T.; Bersie, A.; Wang, Y. C. Extreme Damping in Composite Materials with Negative-Stiffness Inclusions. *Nature* **2001**, *410*, 565–567.